Catena 215 (2022) 106300

Contents lists available at ScienceDirect

Catena

journal homepage: www.elsevier.com/locate/catena

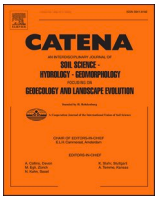

Incorporating ECOSTRESS evapotranspiration in a paired catchment water balance analysis after the 2018 Holy Fire in California

Brenton A. Wilder [a,b], Alicia M. Kinoshita [a,*]

[a] Department of Civil, Construction, and Environmental Engineering, San Diego State University, CA, USA
[b] Department of Geosciences, Boise State University, Idaho, USA

ARTICLE INFO

Keywords:
Ecohydrological Processes
Semi-arid Environment
Remote Sensing
Soil Burn Severity

ABSTRACT

Ecohydrological processes such as evapotranspiration (ET) and streamflow are highly variable after fire in Mediterranean systems and require accurate assessments to improve long-term risk mitigation of erosion and peak flows and revegetation strategies, especially at the small catchment scale. Using the case of the 2018 Holy Fire in southern California, we characterized 1) pre-fire rainfall and evapotranspiration conditions and 2) recovery of ecohydrological processes using a paired analysis between an unburned (Santiago) and burned (Coldwater) catchment. ECOsystem Spaceborne Thermal Radiometer Experiment on Space Station (ECOSTRESS), Operational Simplified Surface Energy Balance Model (SSEBop), vegetation indices, and local rainfall-runoff data were used to characterize the sites and investigate spatial and temporal patterns of post-fire ET. Consistent with the drought conditions in California, we observed low precipitation and ET prior to the fire. Additionally, compared to other vegetation types, montane hardwood species were more likely to be classified as high soil burn severity. We also found that the high spatial and temporal resolution of ECOSTRESS provided more information about the general ET patterns. After the fire, ECOSTRESS ET was sensitive to parameters such as slope aspect, soil burn severity, and vegetation species, which has implications for post-fire vegetation recovery and water storage. This work demonstrates opportunities to apply ECOSTRESS ET across globally diverse ecoregions and small catchment scales to identify potentially high-risk areas and improve fire risk and vegetation recovery assessments.

1. Introduction

Over the past few decades, increasing fire frequency and severity around the globe has posed a concern to the safety and well-being of communities and ecosystems. The 2020 fire season alone burned 16,907 km^2 of land across the state of California and includes the 2020 August Complex Fire (4,179 km^2), which was the largest fire documented in California since 1932 (CALFIRE, 2020). Severe fires such as these affect ecohydrological and geomorphological processes at the catchment scale for several post-fire seasons (Cerdà, 1998; Mayor et al., 2007). There is often an increase in post-wildfire sediment transport (DiBiase & Lamb, 2020) and streamflow (Wine et al., 2018; Wohlgemuth, 2016). Across the burned landscape other processes such as decreases in vegetation root water uptake (Obrist et al., 2004), infiltration rates (Cerdà, 1998), and annual above-ground biomass accumulation (Uyeda et al., 2015) can occur. The normalization of these hydrologic processes in Mediterranean systems, such as catchments of southern California, are relatively resilient after fire and recover within a decade (Wittenberg et al., 2007). However, recovery tends to vary spatially and temporally across different landscapes with respect to soil burn severity, slope aspect, vegetation type, and management intervention such as revegetation and risk mitigation strategies (Fernández & Vega, 2016; Keeley & Keeley, 1981; Kinoshita & Hogue, 2011; Viera et al., 2015; Vo & Kinoshita, 2020; WERT, 2018).

There may also be a notable decrease in evapotranspiration (ET) rates for burned areas in semi-arid regions (Prater & DeLucia, 2006; Poon & Kinoshita, 2018), which has implications for water yield (Kinoshita & Hogue, 2015; Soulis et al., 2021). To date, post-fire ET research and the ecohydrological recovery are limited to plot- and fire-scale investigations (Prater & DeLucia, 2006; Poon & Kinoshita, 2018). At the plot-scale, Prater et al. (2006) coupled energy flux station data (Bowen ratio-energy balance method) with vegetation indices to demonstrate conversion of native sagebrush to invasive grasses in a semi-arid environment after disturbances such as wildfire. Conversion

* Corresponding author at: Department of Civil, Construction, and Environmental Engineering, 5500 Campanile Drive, San Diego, CA 92182-1326, USA.
E-mail address: akinoshita@sdsu.edu (A.M. Kinoshita).

https://doi.org/10.1016/j.catena.2022.106300
Received 19 April 2021; Received in revised form 9 March 2022; Accepted 9 April 2022
Available online 23 April 2022

led to relatively lower soil moisture and ET during the dry months. Another plot-scale study of the 2009 Black Saturday Fires in southern Australia noted a 41% reduction in ET between burned and unburned eucalypt forests one to three years following the fire (Nolan et al., 2014). Nolan et al. (2014) statistically modeled the error of total annual ET and observed the greatest magnitude in error (50%) in the most severely burned forested areas. There is a proportional increase in uncertainty of post-fire ET with burn severity, which highlights the high spatial heterogeneity present even at relatively small plot-scales. At a larger scale (fire size), Poon & Kinoshita (2018) used Operational Simplified Surface Energy Balance Model (SSEBop) monthly ET (ET_{SSEBop}) at 1 km spatial resolution to assess vegetation recovery patterns for a semi-arid region affected by the 2011 Las Conchas Fire in New Mexico (USA). The authors found a statistically significant decrease in ET_{SSEBop} following the fire in 2011 to 2014, which suggested a potential shift in vegetation type from conifer to grasslands. Montes-Helu et al. (2009) observed similar trends in burned versus unburned plots of ponderosa pine forests in northern Arizona (USA) ten years after the 1996 Horseshoe-Hochderffer Fires. This conversion from pine forests to grasslands in the burned area led to decreased sensible heat, latent heat, and net radiation, translating to 16.7% lower peak daily ET rates (Montes-Helu et al., 2009).

The small catchment scale, between plot- and fire-scale, is missing from the current post-fire ET studies. This scale is crucial in post-fire land management, as post-fire effects such as increased peak flow rates occur disproportionately in smaller catchments (Keller et al., 1997; Neary et al., 2005). Studies such as Neary et al. (2005) observed relatively large flows, averaging about 193 cms/km^2 in small catchments (<1 km^2) throughout the western United States. Accurately monitoring vegetation recovery and associated ecohydrological processes (i.e., rainfall-runoff and ET) at this scale will increase our ability to understand and predict the long-term impacts to downstream water resources infrastructure, trails and roads, ecosystems, and communities after fire. High resolution remote sensing measurements provide an opportunity to bridge this knowledge gap. For example, ECOsystem Spaceborne Thermal Radiometer Experiment on Space Station (ECOSTRESS) Jet Propulsion Laboratory Priestley-Taylor (PT-JPL) ET ($ET_{PT\text{-}JPL}$) presents improved spatial (70 m) and temporal resolution (1 to 5 days) for monitoring global vegetation. Global and local ground validations of $ET_{PT\text{-}JPL}$ yielded high correlations (R^2) of 0.88 (Fisher et al., 2020) and 0.89 (Kohli et al., 2020), respectively.

This research builds upon previous studies by incorporating higher resolution ET to assess disturbance from fire in small catchments, which is vital in post-fire land management (USFS, 2020). The overarching goal of this work is to improve post-fire ecohydrological assessments through the integration of high resolution $ET_{PT\text{-}JPL}$ with rainfall-runoff measurements. Using the case of the 2018 Holy Fire, we characterize the typical pre-fire annual rainfall and ET fluctuations and compare spatial and temporal patterns of post-fire ET using a paired catchment approach. Additionally, ET_{SSEBop}, vegetation species type, and soil burn severity classifications were incorporated into our study to interpret these changes.

2. Materials and methods

2.1. Study area and hydrologic data

The study area is located within Orange County and Riverside County, California (USA) and is within the Cleveland National Forest and Santa Ana Mountains (Fig. 1). This region is characterized by a Mediterranean climate, Köppen Csa, which consists of hot, dry summers and cool, mild winters (Peel et al., 2007). While the area is predominantly a chaparral ecosystem, there are also montane hardwood species at higher elevations, where elevations of the study area range from 385 to 1,735 m above mean sea level (msl). The summer dry season occurs

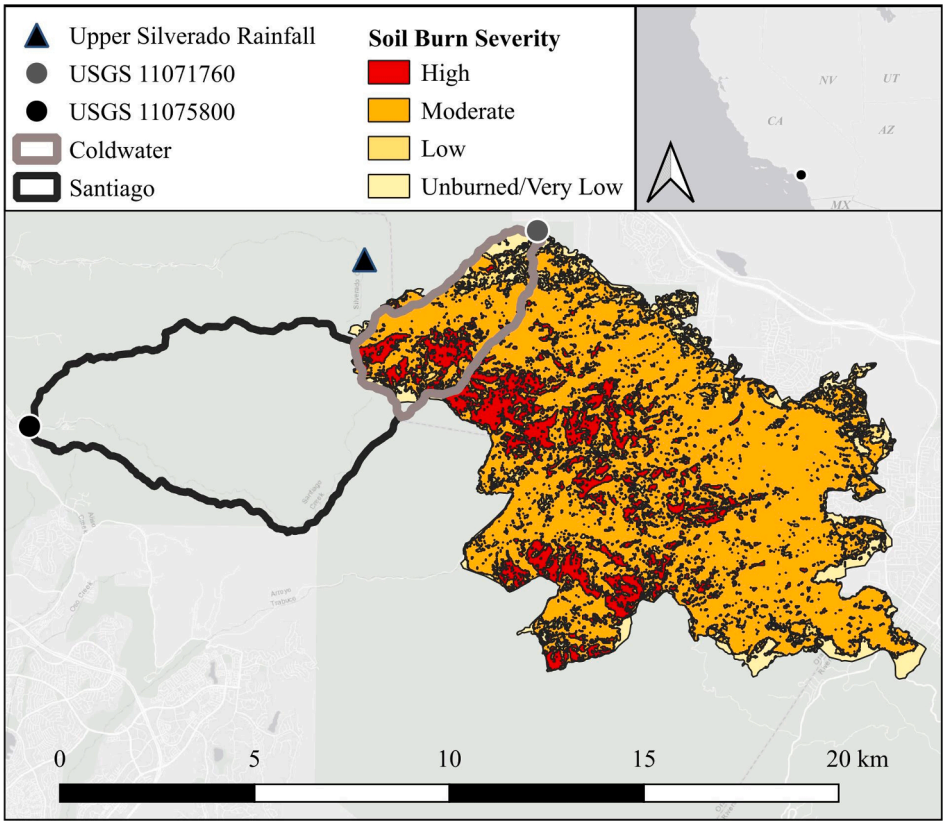

Fig. 1. Locations of Santiago (unburned) and Coldwater (burned) catchments, the 2018 Holy Fire soil burn severity, streamflow (USGS gages 11075800 and 11071760), and precipitation (Upper Silverado rainfall station). The inset shows the general location of the study area in California, United States.

generally between May to October and the winter season occurs November through April. On August 6, 2018, a human-ignited fire burned approximately 94 km^2 (Fig. 1). The soil burn severity classifications for this fire were approximately 14% high, 71% moderate, 8% low, and 7% low to unburned (WERT, 2018). It is noted that the 2020 Bond Fire, burned the foothills approximately 20 km northwest of the Holy Fire. However, this fire occurred almost entirely outside of the study area, thus minimally impacting our analysis.

Two catchments, Santiago (unburned) and Coldwater (burned), were selected for a paired analysis. Studies that utilize an unburned catchment as a reference to a burned catchment are common in post-fire analyses to evaluate the impact of fire (Wagenbrenner et al., 2021). We assumed that differences between the two catchments (streamflow and ET) were due to fire. The neighboring catchments, Santiago and Coldwater, shared a common border and were similar in size, elevation, topography, and vegetation type, consisting of mostly chaparral, coastal scrub, and montane hardwood species (Table 1). Daily streamflow for Santiago and Coldwater were acquired from the United States Geological Survey (USGS) gages 11075800 and 11071760, respectively, for Water Years (WYs) 2019 to 2021 (October 1, 2018 to September 30, 2021). The Coldwater streamgage was installed after the fire on December 4, 2018 and does not have streamflow prior to this date. Streamflow (Q) were transformed to improve the visualization of baseflows in the ephemeral catchments using a Box-Cox transformation (Box & Cox, 1964):

$$Q_{\text{Box-Cox}} = \frac{Q^{\lambda} - 1}{\lambda} \quad (1)$$

where $\lambda = 0.3$ was used for semi-arid regions (Hogue et al., 2000). Daily precipitation for WY 1991 to 2021 were acquired from the Orange County Public Works Upper Silverado station. Catchment parameters that can influence hydrologic properties were derived from spatial datasets including United States Geological Survey (USGS) Digital Elevation Models (10 m spatial resolution), United States Department of Agriculture (USDA) Natural Resources Conservation Service's Soil Survey Geographic Database (SSURGO), and California Department of Forestry and Fire Protection (CAL FIRE) Fveg datasets (Wilder et al., 2021).

Table 1
Catchment parameters and vegetation types for Santiago (unburned) and Coldwater (burned).

Parameters	Santiago	Coldwater
Drainage area (km^2)	32.4	10.9
Lowest elevation (msl)	385	389
Highest elevation (msl)	1735	1735
Area with north aspect	22%	40%
Area with east aspect	13%	32%
Area with south aspect	29%	14%
Area with west aspect	36%	14%
Area covered by forest	28%	37%
Area developed (urban)	2%	2%
Hydrologic soil group A	1%	3%
Hydrologic soil group B	3%	1%
Hydrologic soil group C	9%	0%
Hydrologic soil group D	87%	96%
Average Erodibility Factor (k)	0.3	0.3
Mean slope	55%	63%
Vegetation Type	**Santiago**	**Coldwater**
Mixed Chaparral	65%	54%
Coastal Scrub	14%	8%
Chamise-Redshank Chaparral	8%	2%
Montane Hardwood	7%	31%
Coastal Oak Woodland	3%	4%
Annual Grassland, Barren, Lacustrine, Montane Chaparral, Sierran Mixed Conifer, Urban, and Valley Foothill Riparian	< 3%	< 1%

2.2. Spatial and remote sensing products

The following spatial products were used to characterize the landscape: CAL FIRE Fveg, Environmental Protection Agency (EPA) NHDPlusV2 (National Hydrography Dataset) flow accumulation raster, and U.S. Forest Service soil burn severity map (Table S.1). The CAL FIRE Fveg was compiled from 1990 to 2014 and used to characterize the vegetation species of the study area. The Fveg dataset is the most detailed vegetation classification for California, containing different species found in the region at 30 m spatial resolution (CALFIRE-FRAP, 2015). A flow accumulation raster was acquired from the EPA to define the riparian and hillslope areas of the Holy Fire at 30 m spatial resolution (McKay et al., 2015). The flow accumulation raster was extracted for the fire area and a minimum threshold of 1,500 upstream pixels was used to establish a stream network. Following reclassification and vectorization of the stream network, a 70 m buffer was placed around the stream network to approximate the riparian areas. This buffer was based on the 70 m footprint of ECOSTRESS products and is within optimal vegetative buffers of approximately 100 m to support wildlife habitat (Wenger & Fowler, 2000). A soil burn severity map was acquired from the U.S. Forest Service Burned Area Emergency Response (BAER) Imagery Support. Soil burn severity maps were delineated into four categories (high, moderate, low, and unburned to very low) based on differences in near and mid infrared reflectance values (Parsons et al., 2010). The relation between the pre-fire vegetation type (CAL FIRE Fveg) and soil burn severity were estimated for the Holy Fire extent.

The SSEBop monthly ET, ECOSTRESS Level 3 PT-JPL daily ET, and OpenET are remotely sensed ET products used in this investigation. The SSEBop product is based on the conversion of reference ET to actual ET through the formulation of ecophysiological parameters (land surface temperature, vegetation indices, hot/cold pixels) into a simplified radiation driven energy model (Savoca et al., 2013). Chen et al. (2016) compared ET_{SSEBop} predictions to 42 AmeriFlux sites across the United States from 2001 to 2007, yielding high performance metrics, where R^2 was 0.86 and root mean square error (RMSE) was 15 mm/month (sample size = 1,680). In our study, monthly ET_{SSEBop} at 1 km spatial resolution were collected from WY 2001 to 2021.

ECOSTRESS ET derived from the PT-JPL algorithm ($ET_{PT\text{-}JPL}$) were acquired for July 2018 to October 2021 using the Land Processes Distributed Active Archive Center (LP DAAC) Application for Extracting and Exploring Analysis Ready Samples (AppEEARS) and were processed according to the workflow in Figure S.2. The PT-JPL algorithm is derived using a series of ecophysiological scalar functions based on atmospheric vapor pressure deficit, relative humidity, and vegetation indices to translate potential ET into actual ET (Fisher et al., 2020). $ET_{PT\text{-}JPL}$ data was converted from W/m^2 to mm/day using the latent heat of vaporization and density of water at 20 °C and variable direct sunlight hours (Li et al., 2010). Sunlight hours for the area of the Holy Fire ranged from 7 to 12 h based on the time of year (World Weather and Climate, 2022.). $ET_{PT\text{-}JPL}$ data were also checked for quality using the accompanying ECOSTRESS L3/L4 Ancillary Data Quality Assurance (QA) Flags. No data were withheld for QA flags. However, ten images, which were collected for August 26, 2018, August 23, 2019, September 23, 2019, April 22, 2020, May 20, 2020, June 23, 2020, July 10, 2020, August 21, 2020, May 5, 2021, and June 7, 2021, had $ET_{PT\text{-}JPL}$ that were greater than 3 standard deviations. The ten images were removed, leaving 124 images for our analysis. The ECOSTRESS mission launched on June 29, 2018, thus, limiting the availability for pre-fire analysis. Thus, lower resolution, ET_{SSEBop}, was used to provide a baseline for ET in the study area prior to the Holy Fire.

Finally, PT-JPL derived ET were also collected from the OpenET web platform ($ET_{PT\text{-}JPL\ (OpenET)}$) for our paired study (Melton et al., 2021). The primary forcing data for $ET_{PT\text{-}JPL\ (OpenET)}$ is Landsat TM/ETM+/OLI, while the primary forcing data $ET_{PT\text{-}JPL}$ is from the ECOSTRESS mission. $ET_{PT\text{-}JPL\ (OpenET)}$ is modeled both at the grid scale and farm plot scale (1000 ha limit). For our study, we selected the 30 m grid product for

comparison to the ECOSTRESS ET dataset. Using a dense network of ancillary weather data, remote sensing, and reference ET data, Melton et al. (2021) provide an ensemble of ET model outputs at monthly resolution for applications in the western United States. $ET_{PT\text{-}JPL\ (OpenET)}$ has been ground validated to flux tower agricultural sites in California with R^2 ranging from 0.91 to 0.96 and RMSE ranging from 16 to 26 mm/month. There are no existing flux towers for the Holy Fire area, thus ground validation for our study is not possible. Therefore, we utilized the well tested $ET_{PT\text{-}JPL\ (OpenET)}$ for comparison with data generated from ECOSTRESS ET.

2.3. Local precipitation patterns

A standardized precipitation index (SPI) analysis noted climate anomalies or patterns in the study area (Bonaccorso et al., 2003; World Meteorological Organization, 2012). Daily rainfall data from the Upper Silverado rainfall station, from WY 1991 to 2021, were used to calculate annual SPI using the following equation:

$$\mathrm{SPI} = \frac{P_y - \overline{P}}{\overline{\sigma}} \tag{2}$$

where y denotes the year of interest, P_y is the annual precipitation for a year, and $\overline{P}$ and $\overline{\sigma}$ are the long-term average and standard deviation, respectively. SPI values were classified as follows: greater than 2.0 were extremely wet, between 1.5 and 1.99 were very wet, between 1.0 and 1.49 were moderately wet, between −0.99 to 0.99 were near normal, between −1.0 to −1.49 were moderately dry, between −1.5 to −1.99 were severely dry, and less than −2.0 were extremely dry (World Meteorological Organization, 2012).

2.4. Ecohydrological analyses

2.4.1. Moving average ET model to estimate the post-fire water balance

ECOSTRESS provides estimates of daily ET with variable revisit rates aboard the International Space Station (1–5 days). Annual products are needed to calculate annual water budgets to understand changes in the post-fire hydrology. Due to missing days and the need to smooth variations in the data, ET at the daily scale were approximated for each catchment using a 60 day rolling average algorithm in the Python Pandas package (Reback et al., 2020). This package has a moving window function that calculates a median value for each date based on the values within the specified range (in our case, 60 days). The 60 day window was selected based on the minimum window to build a continuous estimate of evapotranspiration without gaps in the function. The resulting daily ET from the moving average model ($ET_{PT\text{-}JPL,MA}$) were summed to estimate annual ET. To confirm the interpolated moving average results derived from ECOSTRESS, aggregated monthly $ET_{PT\text{-}JPL,MA}$ were compared to $ET_{PT\text{-}JPL\ (OpenET)}$ for Santiago and Coldwater. Due to the size limitation of 1000 ha, we made a representative subsample to approximate $ET_{PT\text{-}JPL\ (OpenET)}$ for each catchment. This validation was carried out for the entire period of record available for the two datasets, July 2019 through July 2021.

Annual $ET_{PT\text{-}JPL,MA}$ was used in a water balance calculation (Figure S.1) to estimate differences in catchment storage volumes for WYs 2020 and 2021:

$$\Delta S = \Delta R + \Delta ET + \Delta G + \Delta P \tag{3}$$

where ΔS is the annual difference in storage between Santiago (unburned) and Coldwater (burned), ΔR is the annual difference in runoff, ΔET is the annual difference between Coldwater and Santiago $ET_{PT\text{-}JPL,MA}$, ΔG is the annual difference in groundwater contribution, and ΔP is the annual difference in rainfall. As the catchments were adjacent and shared similar watershed properties (such as high relief and rainfall), we assumed the differences in groundwater and rainfall between Santiago and Coldwater were minimal, thus ΔG and ΔP approximated as 0.

2.4.2. Spatial and temporal analysis of ET

Google Earth Engine (GEE), a cloud computing platform, was used to analyze spatial trends and create a time series for the satellite-based products (Gorelick et al., 2017). The GEE median reducer function was used to estimate $ET_{PT\text{-}JPL}$, without utilizing the moving average model described previously, from each scene for the spatial datasets (i.e., aspect and vegetation). Average $ET_{PT\text{-}JPL}$ were compiled for WY 2019, 2020, and 2021 to analyze post-fire spatial and temporal trends with respect to vegetation types, slope aspect, soil burn severity, riparian/hillslope areas. Additionally, we identified four images from similar dates (first week of August) to compare the distribution of $ET_{PT\text{-}JPL}$ between Coldwater and Santiago across four years (pre-fire, 1 year post-fire, 2 years post-fire, and 3 years post-fire). We plotted relative density histograms and used common statistics such as two sample t-tests, means, and interquartile ranges to compare differences in the distributions.

3. Results

3.1. Local precipitation patterns and ET processes

Annual SPI (WY 1991 to 2021) and SSEBop ET (WY 2001 to 2021) were calculated for the Holy Fire burn scar (Fig. 2). Wet years appeared intermittently, typically after four to six moderately dry to normal years. No years had an SPI greater than 1.0 in 2012 to 2018 (no wet years), highlighting the seven year drought period prior to the fire. This extended dry period is documented as a period of extreme drought that caused widespread plant stress across northern and southern California (Dong et al., 2019). Immediately following the fire, in WY 2019, a moderately wet year occurred (SPI = 1.20; Fig. 2). WY 2019 featured several strong storms, with 15 min rainfall intensities measuring as high as 32 mm/hr (Guilinger et al., 2020).

Due to the product availability and resolution, evapotranspiration was estimated from SSEBop for the Holy Fire area from WY 2001 to 2017 (pre-fire). The average annual pre-fire ET_{SSEBop} was 722 mm for the entire area and ranged from 610 to 947 mm (Fig. 2). The three years prior to the fire had the lowest ET, ranging from 610 to 625 mm. Additionally, all seven years prior to the fire were below the pre-fire average. A modest correlation existed between pre-fire annual ET_{SSEBop} and SPI ($R^2 = 0.64$; n = 17), where generally the extreme wet and dry years had relatively high ET_{SSEBop} (i.e., 947 in WY 2005) and low ET_{SSEBop} (i.e., 678 in WY 2007), respectively. After the fire in 2019, there was a moderately wet year, which had 1,036 mm of rainfall, resulting in a large resurgence in ET_{SSEBop} (44% increase) the following year in WY 2020 (Fig. 2).

Focusing on the seven year drought period (WY 2012 to 2018), we compared the monthly ET_{SSEBop} to the eleven years (WY 2001 to 2011) prior to the drought that contained two moderately wet years, two moderately dry years, and seven near normal years. This period encompassed typical cyclical climate fluctuations associated with El Niño-Southern Oscillation patterns. The two groups were statistically

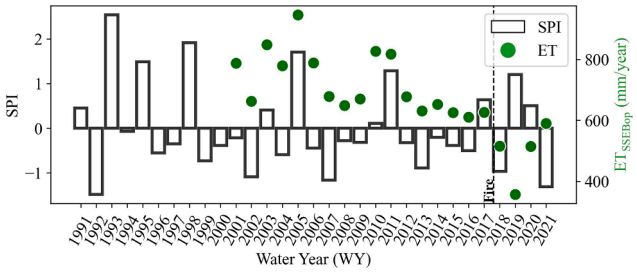

Fig. 2. Annual Standardized Precipitation Index (SPI) for WY 1991 to 2021 and ET_{SSEBop} for WY 2001 to 2021 for the area affected by the Holy Fire. The approximate date (August 2018) of the fire is denoted by a vertical dashed line.

different ($p < 0.05$) for all months (except November), where the seven year drought period before the fire had significantly lower ET_{SSEBop} (Fig. 3). Across the entire pre-fire period (2000 to 2018), monthly ET_{SSEBop} typically peaked in this region during the dry period between June to July, with values ranging from 64 to 151 mm/month. Most notably, one month prior to the fire in July of WY 2018, ET_{SSEBop} was 64 mm/month, the lowest value for the pre-fire record (2001 to 2018) for the month of July.

3.2. Pre-fire vegetation type and soil burn severity

Soil burn severity categories were differentiated by pre-fire vegetation type for the entire Holy Fire landscape (Fig. 4). Montane hardwood had the greatest proportion (33%) of high soil burn severity for all vegetation types. This was followed by 12% of mixed chaparral and < 1% of coastal scrub that burned at high soil burn severity. The majority of the Holy Fire was classified as moderate soil burn severity, which was the most common soil burn severity for all vegetation types. Mixed chaparral had the highest proportion (75%) of moderate soil burn severity for all vegetation types. This was followed by 62% of coastal scrub and 60% of montane hardwoods at moderate soil burn severity. Finally, 37% of coastal scrub were classified as low (23%) and very low to unburned (14%) soil burn severity.

3.3. Post-fire paired catchment analysis

The post-fire ecohydrological patterns for the two catchments were different from WY 2019 to WY 2021 (Fig. 5). The differences between the two catchments were sinusoidal after the fire, where the greatest difference in magnitude (1 to 2 mm/day) between the unburned and burned catchments occurred during the dry months and the smallest difference (0 to 1 mm/day) during the winter months. The runoff events in the winter were also larger in magnitude for the burned catchment (Fig. 5c). For example, the December 6, 2018, storm generated 55 mm of rainfall, which translated to a daily average runoff of 1.6 mm for Coldwater (burned) and 0.02 mm for Santiago (unburned). The following year, a storm on November 28, 2019, generated 74 mm of rainfall, which translated to a daily average runoff of 1.4 mm and 0.28 mm for Coldwater and Santiago, respectively. The third year after fire (WY 2021) was a severe drought year, with only 92 mm of annual rainfall, and therefore, no noteworthy runoff events were observed.

We approximated a continuous estimate of $ET_{PT\text{-}JPL}$ ($ET_{PT\text{-}JPL,MA}$) for the second (WY 2020) and third (WY 2021) post-fire years (Fig. 5b; Table 2). Using $ET_{PT\text{-}JPL,MA}$, we constructed a simple water balance model (Equation (3)) to estimate the ΔS between the paired catchments.

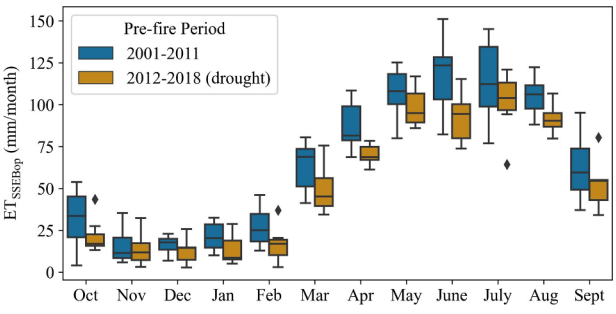

Fig. 3. Pre-fire average monthly SSEBop evapotranspiration (ET_{SSEBop}) for the 2018 Holy Fire burned area for the pre-drought period (WY 2001 to 2011; blue) and the drought period immediately preceding the Holy Fire (WY 2012 to 2018; brown). Note that the average number of pixels in the burned area is 103 and WY 2018 does not include the immediate post-fire months of August and September. Outliers are denoted by solid diamonds. (For interpretation of the references to colour in this figure legend, the reader is referred to the web version of this article.)

The annual precipitation for the study area was 1036, 774, and 97 mm for 2019, 2020, and 2021, respectively. The difference in runoff, ΔR, in WY 2020 was 131 mm, indicating more direct runoff for the burned catchment. This was a 128% increase in annual direct runoff compared to the streamflow for the unburned catchment during the same year. The difference in $ET_{PT\text{-}JPL,MA}$, ΔET, in the second post-fire WY was −215 mm, indicating a decrease in $ET_{PT\text{-}JPL}$ for the burned catchment. The difference in storage, ΔS, was + 85 mm, suggesting more storage in the burned catchment. For WY 2021, ΔR was 59 mm, indicating more direct runoff for the burned catchment, despite the exceptionally dry conditions. The difference in $ET_{PT\text{-}JPL,MA}$, ΔET, in the third post-fire WY was −140 mm, suggesting a decrease in $ET_{PT\text{-}JPL}$ for the burned catchment. The difference in storage, ΔS, was + 80 mm, which suggested more storage in the burned catchment relative to the unburned catchment.

3.4. Validating the moving average model with OpenET

We also compared monthly $ET_{PT\text{-}JPL,MA}$ to $ET_{PT\text{-}JPL(OpenET)}$ between July 2019 to July 2021 (Fig. 6). There was an adequate agreement between the two estimates for both burned ($R^2 = 0.64$; RMSE = 13 mm/month) and unburned ($R^2 = 0.69$; RMSE = 19 mm/month) catchments. On average there is a slight negative bias of $ET_{PT\text{-}JPL,MA}$ compared to $ET_{PT\text{-}JPL(OpenET)}$ (Bias = -12 mm/month). $ET_{PT\text{-}JPL(OpenET)}$ had decreased ET for all seasons, with the most pronounced differences during the growing season. For example, during the first post-fire year, monthly ET production was reduced by nearly half compared to the unburned catchment. This is also represented in the moving average model derived from ECOSTRESS data and supports significant decreases in post-fire ET.

3.5. Spatial and temporal recovery of ET

We compared the average $ET_{PT\text{-}JPL}$ for each water year from October 2018 to October 2021 (124 images). Average annual $ET_{PT\text{-}JPL}$ varied with respect to landscape subgroups: slope aspect, soil burn severity, riparian/hillslope, and pre-fire vegetation species (Table 3). Most notably for WY 2019, the montane hardwood species in higher elevations had the largest average $ET_{PT\text{-}JPL}$ for the first year after fire. In WY 2019, the $ET_{PT\text{-}JPL}$ varied minimally by soil burn severity (+/- 0.01 to 0.02 mm/day), suggesting relatively homogeneous conditions across the burned landscape during the first year. Spatial heterogeneity increased during the second and third post-years, where standard deviations of the burned landscape sub-groups were 0.08 mm/day, 0.09 mm/day, and 0.14 mm/day for WY 2019, WY 2020, and WY 2021, respectively. For WY 2020, there was a similar relationship, where areas containing montane hardwood species before the fire exhibited the highest $ET_{PT\text{-}JPL}$ production (2.44 mm/day) of all the vegetation subgroups. In the second year after fire, the high soil burn severity areas had the second most $ET_{PT\text{-}JPL}$ production (2.37 mm/day) of the burned subgroups. It appeared that areas of west facing slopes (towards the ocean) had the highest $ET_{PT\text{-}JPL}$ production (2.35 mm/day) during the second year after the fire. There was also a slight decrease in $ET_{PT\text{-}JPL}$ in WY 2020. Finally, high soil burn severity, north and west facing slopes, and montane hardwood areas produced the most $ET_{PT\text{-}JPL}$ out of all landscape subgroups.

Relative density histograms for four dates (August 2, 2018 (pre-fire), August 1, 2019, August 1, 2020, and August 7, 2021) had a similar pattern of lower $ET_{PT\text{-}JPL}$ for Coldwater compared to Santiago (Fig. 7). The shifts over time and between watersheds were not statistically significant. However, the means and spread of the ET data highlights differences in the distribution of the data. Similar $ET_{PT\text{-}JPL}$ patterns were observed between Coldwater (1.63 mm) and Santiago (1.54 mm) before the fire (Fig. 7a). There was spatial heterogeneity and complexity present prior to the fire, which was represented by an interquartile range (IQR) of 0.70 mm in Coldwater. One year after the fire (2019), the mean $ET_{PT\text{-}JPL}$ (0.90 mm) and IQR (0.25 mm) in Coldwater decreased abruptly (Fig. 7b); while the mean $ET_{PT\text{-}JPL}$ in Santiago was 2.34 mm. This

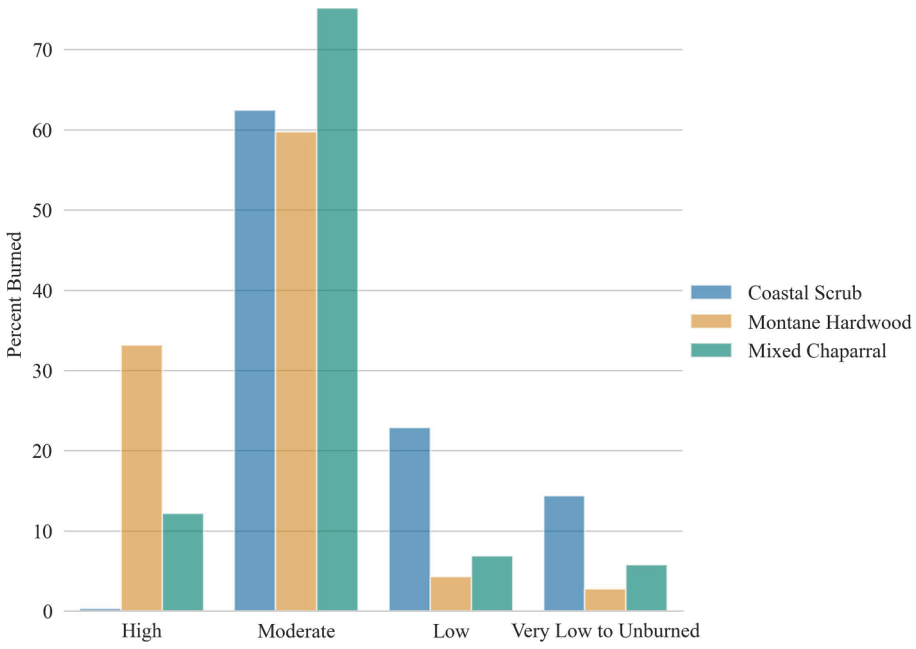

Fig. 4. The proportion of soil burn severity for each of the pre-fire vegetation types for the area burned by the Holy Fire.

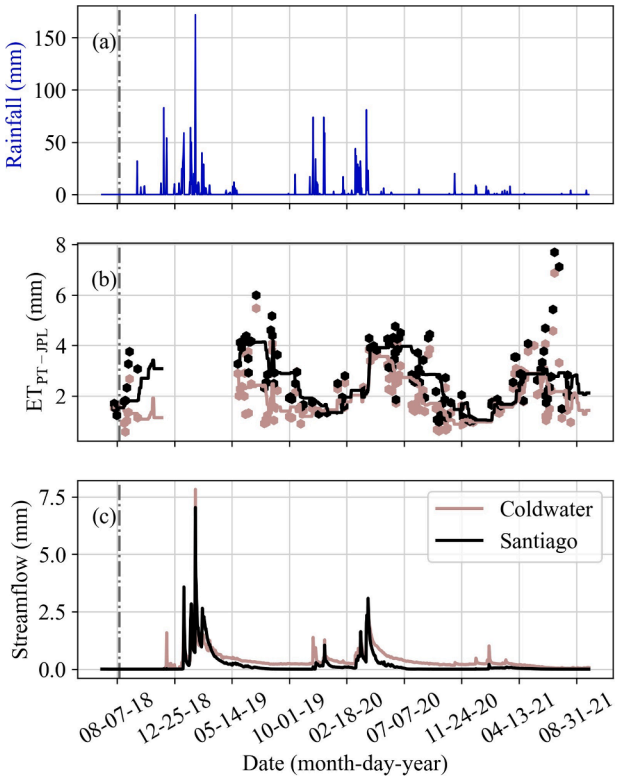

Fig. 5. Daily rainfall (a), daily evapotranspiration (ET_{PT-JPL}), where the 60 day moving average ET model ($ET_{PT-JPL,MA}$) for Coldwater (burned) and Santiago (unburned) are denoted as solid lines (b), and daily streamflow (c) for Coldwater and Santiago from WY 2019 to 2021. A grey dashed vertical line on each subplot denotes the 2018 Holy Fire.

Table 2
Annual ECOSTRESS ET ($ET_{PT-JPL,MA}$), precipitation (P), and runoff (R) for the burned and unburned catchments.

	Coldwater (burned)		Santiago (unburned)	
WY	$ET_{PT-JPL,MA}$ (mm)	R (mm)	$ET_{PT-JPL,MA}$ (mm)	R (mm)
2019*	NA	279	NA	256
2020	779	233	994	102
2021	617	66	757	6

NA – data unavailable due to the data outage of ECOSTRESS.
* Runoff data for WY 2019 were not available prior to December 4, 2018. Runoff data after December 4, 2018 were used for both catchments.

indicates homogenous conditions initially after the fire in addition to decreased ET_{PT-JPL}. Similarly, a large reduction in mean ET_{PT-JPL} was observed in the second (2020) and third post-fire years (2021). In August 2020, Coldwater and Santiago had a mean ET_{PT-JPL} of 1.39 mm and 2.56 mm, respectively, and the third post-fire year had a mean ET_{PT-JPL} of 1.50 mm and 2.12 mm in Coldwater and Santiago, respectively.

Finally, we compared ET_{PT-JPL} images before (August 2, 2018) and three years after fire (August 7, 2021). Large areas of low ET_{PT-JPL} were more prevalent in 2021. This was especially noticeable in the northwestern edge of the burned area (Fig. 8b and d), where areas defined as montane hardwood species before the fire had comparatively less ET_{PT-JPL}, approximately 17% reduction, between August 2018 and August 2021.

4. Discussion

4.1. Pre-fire drought conditions

Prior to the fire, the local precipitation patterns in WYs 2012 to 2016 and 2018 ranged from normal to moderately dry (Fig. 2), which coincided with a drought period throughout the state of California (Dong et al., 2019). Compared to other vegetation types in the study area,

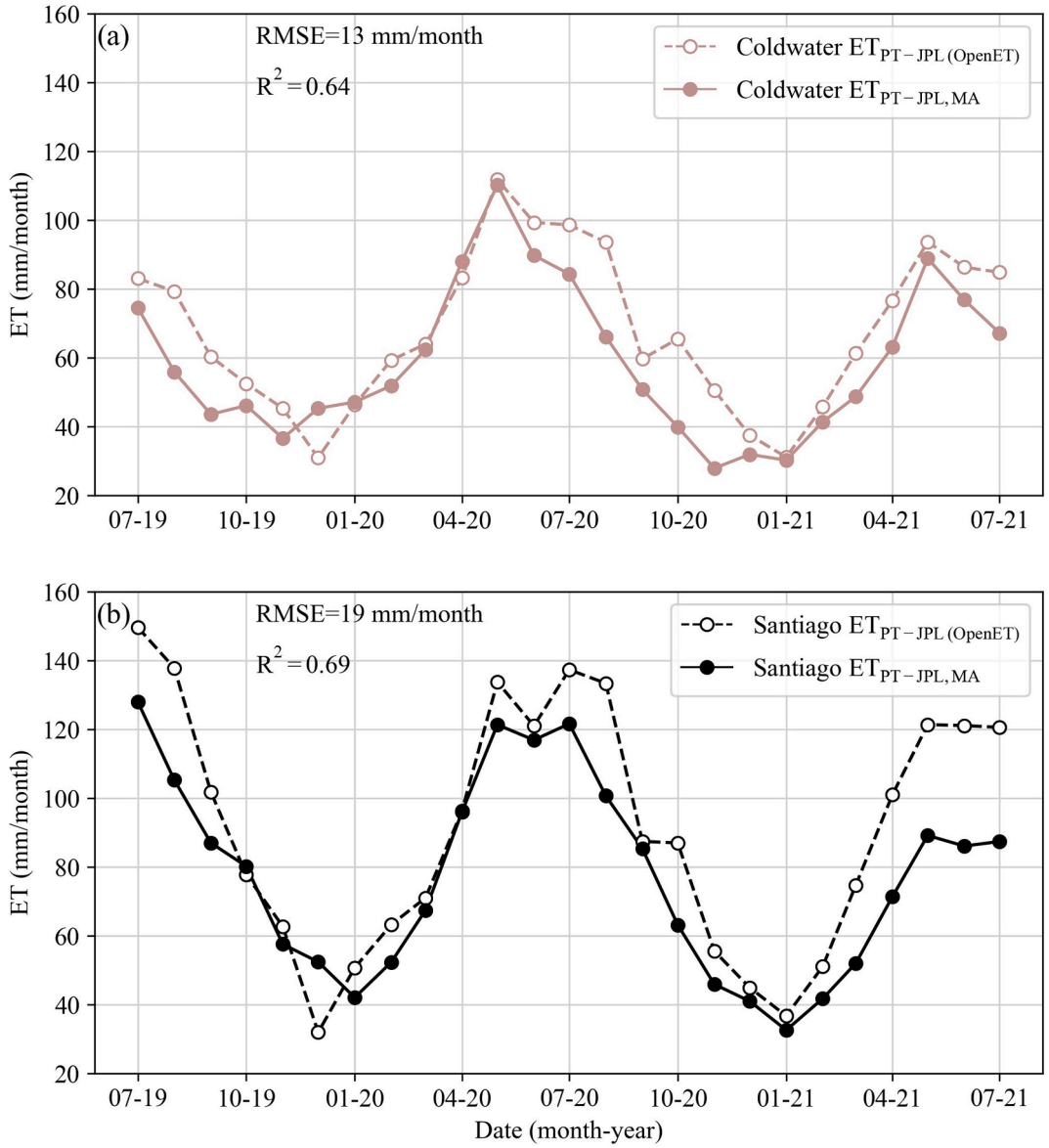

Fig. 6. Monthly comparison of $ET_{PT\text{-}JPL,MA}$ versus $ET_{PT\text{-}JPL\ (OpenET)}$ for (a) Coldwater (burned) and (b) Santiago (unburned) between July 2019 to July 2021.

Table 3
Average $ET_{PT\text{-}JPL}$ for WY 2019, WY 2020, and WY 2021 for the Holy Fire with respect to riparian versus hillslope, soil burn severity, slope aspect, and pre-fire vegetation species. The averages for burned (Coldwater) and unburned (Santiago) catchments are also included for comparison.

Landscape sub-groups	Average $ET_{PT\text{-}JPL}$ (mm/day)		
	WY 2019	WY 2020	WY 2021
Riparian (n = 1,205)	2.00	2.27	2.09
Outside of riparian (n = 17,979)	2.09	2.32	2.10
High (n = 2,743)	2.05	2.37	2.22
Moderate (n = 13,563)	2.05	2.31	2.09
Low (n = 1,477)	2.03	2.17	1.89
North (n = 7,014)	2.04	2.32	2.18
East (n = 5,019)	2.00	2.28	2.05
South (n = 4,251)	1.99	2.31	2.03
West (n = 2,900)	2.07	2.35	2.16
Mixed Chaparral (n = 12,878)	2.06	2.32	2.09
Montane Hardwood (n = 3,000)	2.14	2.44	2.28
Coastal Scrub (n = 1,038)	1.82	2.09	1.75
Coldwater (n = 2,224)	2.33	2.28	2.07
Santiago (n = 6,612)	3.50	3.01	2.55

montane hardwood species had the largest proportion of high soil burn severity. Montane hardwood species are typically well adapted to drought, however, can experience high water stress and tree mortality during long drought periods (Guarín & Taylor, 2005), thus leading to elevated potential for fire (Taylor et al., 2008). Our analysis highlights the impact of the seven year drought, which led to high soil burn severity for regions with large proportions of montane hardwoods. It is also noted that the composition of montane hardwoods in Santiago (unburned) and Coldwater (burned) was 8% and 31%, respectively (Table 1), which was the largest difference between the initial conditions of the paired catchments.

4.2. Post-fire evapotranspiration and storage

We used $ET_{PT\text{-}JPL}$ and Equation (3) to approximate the difference in storage between the unburned and burned catchment to link the runoff measurements to vegetation recovery for WY 2020 and 2021. For WY 2020 and 2021, $\Delta ET_{PT\text{-}JPL,MA}$ was −215 mm and −140 mm, respectively, suggesting decreased ET in the burned catchment relative to the unburned catchment. This was similar to previous studies, which also noted decreased post-fire ET in semi-arid regions (Poon & Kinoshita,

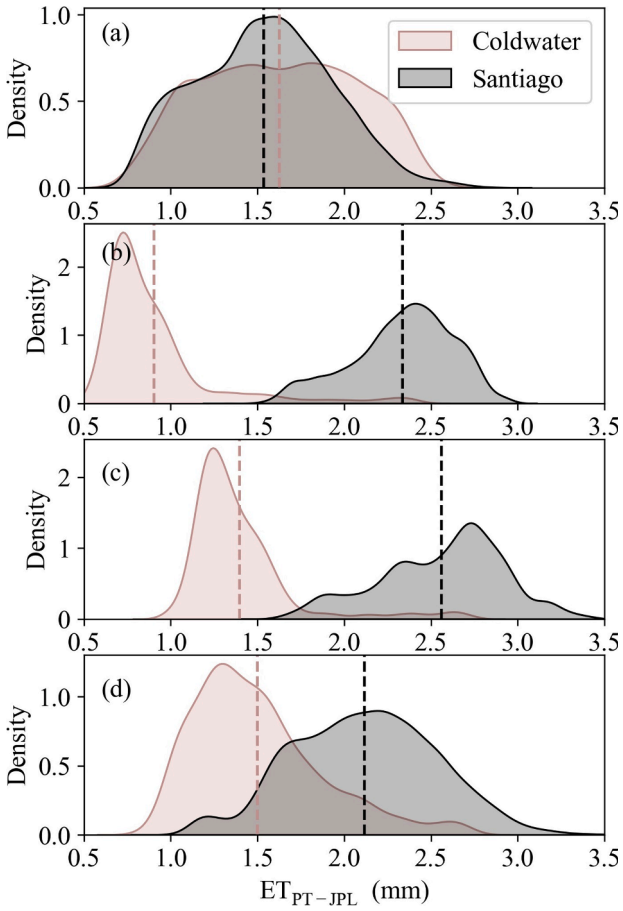

Fig. 7. Relative density histograms of $ET_{PT\text{-}JPL}$ for Coldwater (burned) and Santiago (unburned), for August 2, 2018 (pre-fire; a), August 1, 2019 (b), August 1, 2020 (c), and August 7, 2021 (d). Dashed vertical lines represent the respective means of the distributions.

2018; Prater & DeLucia, 2006; Ma et al., 2020; Nolan et al. 2014; Soulis et al., 2021). The reduction of ET in the burned catchment, coupled with the increase in streamflow, likely contributed to the slight increased soil water storage and is similar to post-fire soil storage conditions documented in semi-arid sites (i.e. Montes-Helu et al., 2009; Atchley et al., 2018).

While we did not conduct ground validation for our study site, we compared monthly $ET_{PT\text{-}JPL(OpenET)}$ to monthly $ET_{PT\text{-}JPL,MA}$ (Fig. 6). The moving average accuracy was sensitive to the calculation of sunlight hours used to transform $ET_{PT\text{-}JPL}$ from units of W/m^2 to mm/day. This was noted by the large bias of 12 mm/month in the model comparison. In this study, sunlight hours were approximated from weather estimates in Los Angeles County, however, future studies should include better local estimates of sunlight hours to improve ET model accuracy (Li et al., 2010). Despite this source of error, there was still a modest correlation with $ET_{PT\text{-}JPL(OpenET)}$, which has better ancillary data. This provides us with confidence in the post-fire water balance calculated with the ECOSTRESS moving average model.

4.3. Post-fire revegetation and recovery strategies after the Holy fire

After the Holy Fire, Burned Area Emergency Response (BAER) treatment recommended strategies to mitigate post-fire risks and promote healthy regrowth. Strategies included identification of noxious weed suppression points or areas, signage and gates to limit access to hazardous areas, hazmat stabilization for residential areas, road stabilization, storm proofing trails, and identification of habitat for threatened species (i.e. California Gnatcatcher, or *Polioptila californica*). Further, suppression of invasive species such as Tamarisk (*Tamarix aphylla*) are crucial for the regrowth of native chaparral. Maintaining native vegetation may prevent invasion of non-native species and shifts in altered fire regimes (Mathews & Kinoshita, 2020). Native vegetation also provides critical habitats for species like the California Gnatcatcher, who's habitat may take up to 10 years to fully recover after fire (BAER, 2018). Finally, drainage infrastructure within the burn scar were maintained and improved to increase performance under more intense runoff conditions and reduce the risk of road and trail failure. Due to the severity of the Holy Fire and safety concerns, the area remained closed to the public until partial reopening in October 2021 (https://www.fs.usda.gov/cleveland/).

We note that satellite-based ET cannot be differentiated between vegetation species that were present before and after fire without field-based validation. However, in this study we demonstrated the reduction in $ET_{PT\text{-}JPL}$ for montane hardwood species at high elevations (Fig. 8). This type of analysis could be useful in future post-fire assessments of sensitive habitats and treatment strategies. For example, large and prevalent patches of low $ET_{PT\text{-}JPL}$ suggested a shift in vegetation composition (i.e., conversion to grasslands). Field photos from Spring 2019 confirm a large resurgence of annual grasses on many slopes in the higher elevations after one year of regrowth following the fire (Figure S.3).

4.4. Application of ECOSTRESS and opportunities for future fire management

Improving our understanding of ecohydrological recovery is relevant for protecting sensitive ecosystems and assessing the potential for flooding and debris flow hazards during the post-fire recovery period. However, most post-fire studies focused on the initial (<5 years) effects of wildfire and few studies investigated the longer-term effects of wildfire (Wagenbrenner et al., 2021), despite the value of long-term research (Tetzlaff et al., 2017). Further, few datasets include pre- and post-fire hydrologic responses from small catchments for periods long enough to make an assessment post-fire response. Thus, the effects of fire are uncertain, creating challenges for predicting catchment processes during the post-fire recovery period and longer-term post-fire management (Wagenbrenner et al., 2021).

This study highlights the importance of higher spatial resolution products such as $ET_{PT\text{-}JPL}$ to advance modeling and prediction of coupled ecohydrological processes at the catchment scale during the post-fire recovery period. We demonstrated the differences between $ET_{PT\text{-}JPL}$ with respect to slope aspect, soil burn severity, riparian/hillslope, and vegetation type (Table 3). The small footprint of $ET_{PT\text{-}JPL}$ adequately captures spatial heterogeneity present in post-fire parameters such as land surface temperature, which are dependent on features such as topography and vegetation. Also, higher soil burn severities typically have the greatest effects on ecohydrological processes and recovery time (Lentile et al., 2007; Parsons et al., 2010). In this study, the $ET_{PT\text{-}JPL}$ production was homogeneous across all landcover types during the first year after fire and became more spatially heterogeneous in the following years (Table 3). However, more work is needed to field validate $ET_{PT\text{-}JPL}$ in post-fire settings across diverse ecoregions and for longer timespans. Additionally, while soil moisture was not within the scope of this work, future studies are encouraged to integrate field observations and measurements of soil moisture to improve our understanding of the water balance and storage dynamics for burned catchments.

While this study is a preliminary presentation of ECOSTRESS, we advocate that the application of high spatial and temporal resolution ECOSTRESS data can supplement and address crucial science questions for future fires. ECOSTRESS provides scientists with higher resolution ET and Evaporative Stress Index data that can improve precision of fire risk analyses. We used a lower resolution product, SSEBop, to observe ET in the pre-fire study period and make general observations about the seasonal ET patterns, where higher resolution data were unavailable.

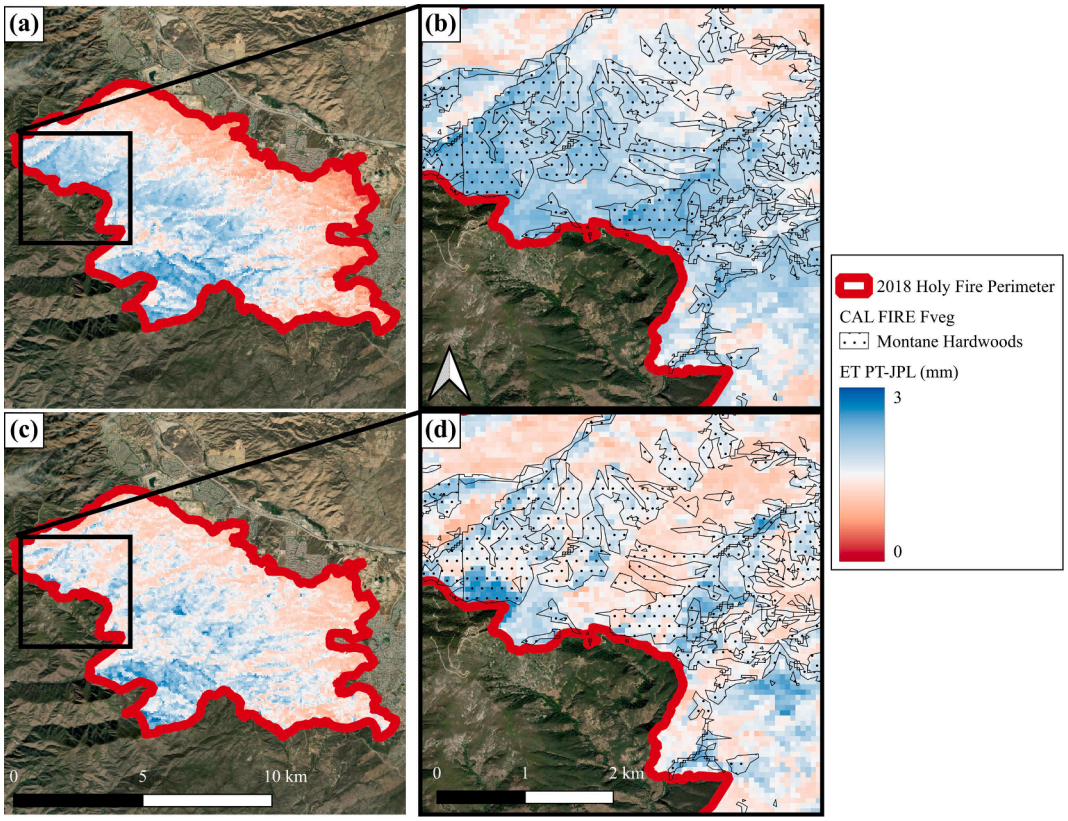

Fig. 8. $ET_{PT\text{-}JPL}$ within the area burned by the 2018 Holy Fire for August 2, 2018 (pre-fire, a) and August 7, 2021 (three years post-fire, c). $ET_{PT\text{-}JPL}$ within the northwestern edge of the burned area for August 2, 2018 (b) and August 7, 2021 (d) with respect to montane hardwood species.

For example, we observed minimum ET_{SSEBop} occurred conjointly with three consecutive years of the lowest annual ETs, due to the combination of severe drought and presumably high water stress conditions. We also demonstrated the application of $ET_{PT\text{-}JPL}$ to quantify the post-fire water budget and partitioning of rainfall-runoff, ET, and net storage, which may help with prioritizing management decisions for small catchments.

Future assessments of small post-fire catchments may become more prevalent by combining field-based and remotely sensed data to determine the impacts of geology, climate, vegetation, and changes in soil structure on recovery of hydrologic processes. Along with ground-based validation efforts, the use of Unmanned Aircraft Systems (UAS) may present an opportunity to improve certainty in post-fire assessments of satellite-based ET (Fernández-Guisuraga et al., 2018). As researchers and managers incorporate and adapt technology such as airborne and satellite imaging advances, we will continue to increase our understanding of post-fire hydrological impacts.

5. Conclusion

Ecohydrological processes such as streamflow and evapotranspiration (ET) are highly variable after fire in Mediterranean systems with respect to time and space, therefore prompting the need for monitoring recovery. In this study, remote sensing products and hydrologic data for Santiago (unburned) and Coldwater (burned) were used to evaluate the effects of the 2018 Holy Fire. The paired catchment analysis allowed us to control for variability in weather and to demonstrate the application of ECOSTRESS to estimate ET for post-fire analysis. The burned areas in the Holy Fire were more likely to be classified as high soil burn severity if the pre-fire area contained montane hardwood species. There was also a sustained decline in ET_{SSEBop} preceding the fire, which was accompanied by low total rainfall during the drought in California (WYs 2012 to 2016 and 2018). This study highlights opportunities for fire managers to utilize ECOSTRESS to identify specific areas that have high evaporative stress and dry conditions conducive to fire. Using ECOSTRESS, we modeled reduced annual totals of post-fire $ET_{PT\text{-}JPL}$ and a small increase in soil water storage. We also highlighted the variability in $ET_{PT\text{-}JPL}$ patterns for land surface features such as slope aspects, soil burn severity, and vegetation species, which was possible at 70 m resolution with ECOSTRESS. This work demonstrates that high resolution products such as daily $ET_{PT\text{-}JPL}$ may be an effective tool for monitoring ecohydrological recovery in small catchments after fire across diverse ecoregions around the globe.

Database

Wilder, B. A., A. M. Kinoshita (2022). Monitoring Fire Severity and Ecohydrological Recovery for the 2018 Holy Fire in Southern California, HydroShare, https://doi.org/10.4211/hs.c54a283dbefa4fa081fa8fcad8d634ca.

Declaration of Competing Interest

The authors declare that they have no known competing financial interests or personal relationships that could have appeared to influence the work reported in this paper.

Acknowledgements

We thank Christine Lee and Paa Sey from NASA JPL for the insightful discussions regarding the use of ECOSTRESS in wildfire applications. We also appreciate Victoria Stempniewicz, Andrew Gray, James Guilinger, and the rest of the United States Forest Service hydrologists and UC Riverside researchers in attendance at the 2020 Holy Fire Research Symposium for sharing updates on the recovery. We are appreciative of

Brian Swanson from the Department of Conservation - California Geological Survey (CGS) for sharing insights and imagery following the 2018 Holy Fire. We also thank two anonymous reviewers and the editors whose insightful comments improved this paper.

Funding

This work was supported by a Joint Fire Science Program Graduate Research Innovation Award (#19-1-01-55) and San Diego State University Master's Research Scholarship Award. This material is also based upon work supported by the National Science Foundation CAREER Program under Grant No. 1848577.

Appendix A. Supplementary material

Supplementary data to this article can be found online at https://doi.org/10.1016/j.catena.2022.106300.

References

Atchley, A.L., Kinoshita, A.M., Lopez, S.R., Trader, L., Middleton, R., 2018. Simulating Surface and Subsurface Water Balance Changes Due to Burn Severity. Vadose Zone Journal 17 (1), 180099. https://doi.org/10.2136/vzj2018.05.0099.

BAER (Burned Area Emergency Response). (2018). Holy Fire— Burned Area Emergency Response, https://www.fs.usda.gov/Internet/FSE_DOCUMENTS/fseprd594859.pdf.

Bonaccorso, B., Bordi, I., Cancelliere, A., Rossi, G., Sutera, A., 2003. Spatial variability of drought: an analysis of the SPI in Sicily. Water resources management 17 (4), 273–296. https://doi.org/10.1023/A:1024716530289.

Box, G.E.P., Cox, D.R., 1964. An Analysis of Transformations. Journal of the Royal Statistical Society: Series B (Methodological) 26 (2), 211–243. https://doi.org/10.1111/j.2517-6161.1964.tb00553.x.

CALFIRE. (Nov, 2020). Top 20 largest California wildfires.

CALFIRE-FRAP. (2015). *Vegetation (fveg) - CALFIRE FRAP [ds1327]*. https://map.dfg.ca.gov/metadata/ds1327.html.

Cerdà, A., 1998. Changes in overland flow and infiltration after a rangeland fire in a Mediterranean scrubland. Hydrological processes 12 (7), 1031–1042. https://doi.org/10.1002/(SICI)1099-1085(19980615)12:7<1031::AID-HYP636>3.0.CO;2-V.

Chen, M., Senay, G.B., Singh, R.K., Verdin, J.P., 2016. Uncertainty analysis of the Operational Simplified Surface Energy Balance (SSEBop) model at multiple flux tower sites. Journal of Hydrology 536, 384–399. https://doi.org/10.1016/j.jhydrol.2016.02.026.

DiBiase, R.A., Lamb, M.P., 2020. Dry sediment loading of headwater channels fuels post-wildfire debris flows in bedrock landscapes. Geology 48 (2), 189–193. https://doi.org/10.1130/G46847.1.

Dong, C., MacDonald, G.M., Willis, K., Gillespie, T.W., Okin, G.S., Williams, A.P., 2019. Vegetation responses to 2012–2016 drought in Northern and Southern California. Geophysical Research Letters 46 (7), 3810–3821. https://doi.org/10.1029/2019GL082137.

Fernández, C., Vega, J.A., 2016. Modelling the effect of soil burn severity on soil erosion at hillslope scale in the first year following wildfire in NW Spain. Earth Surface Processes and Landforms 41 (7), 928–935. https://doi.org/10.1002/esp.3876.

Fernández-Guisuraga, J.M., Sanz-Ablanedo, E., Suárez-Seoane, S., Calvo, L., 2018. Using unmanned aerial vehicles in postfire vegetation survey campaigns through large and heterogeneous areas: Opportunities and challenges. Sensors 18 (2), 586. https://doi.org/10.3390/s18020586.

Fisher, J.B., Lee, B., Purdy, A.J., Halverson, G.H., Dohlen, M.B., Cawse-Nicholson, K., Wang, A., Anderson, R.G., Aragon, B., Arain, M.A., Baldocchi, D.D., Baker, J.M., Barral, H., Bernacchi, C.J., Bernhofer, C., Biraud, S.C., Bohrer, G., Brunsell, N., Cappelaere, B., Castro-Contreras, S., Chun, J., Conrad, B.J., Cremonese, E., Demarty, J., Desai, A.R., De Ligne, A., Foltýnová, L., Goulden, M.L., Griffis, T.J., Grünwald, T., Johnson, M.S., Kang, M., Kelbe, D., Kowalska, N., Lim, J.-H., Maïnassara, I., McCabe, M.F., Missik, J.E.C., Mohanty, B.P., Moore, C.E., Morillas, L., Morrison, R., Munger, J.W., Posse, G., Richardson, A.D., Russell, E.S., Ryu, Y., Sanchez-Azofeifa, A., Schmidt, M., Schwartz, E., Sharp, I., Šigut, L., Tang, Y., Hulley, G., Anderson, M., Hain, C., French, A., Wood, E., Hook, S., 2020. ECOSTRESS: NASA's Next Generation Mission to Measure Evapotranspiration from the International Space Station. Water Resources Research 56 (4). https://doi.org/10.1029/2019WR026058.

Gorelick, N., Hancher, M., Dixon, M., Ilyushchenko, S., Thau, D., Moore, R., 2017. Google Earth Engine: Planetary-scale geospatial analysis for everyone. Remote Sensing of Environment 202, 18–27. https://doi.org/10.1016/j.rse.2017.06.031.

Guarín, A., Taylor, A.H., 2005. Drought triggered tree mortality in mixed conifer forests in Yosemite National Park. Forest Ecology and Management 218 (1-3), 229–244. https://doi.org/10.1016/j.foreco.2005.07.014.

Guilinger, J.J., Gray, A.B., Barth, N.C., Fong, B.T., 2020. The Evolution of Sediment Sources Over a Sequence of Postfire Sediment-Laden Flows Revealed Through Repeat High-Resolution Change Detection. Journal of Geophysical Research: Earth Surface. 125 (10) https://doi.org/10.1029/2020JF005527.

Hogue, T.S., Sorooshian, S., Gupta, H., Holz, A., Braatz, D., 2000. A multistep automatic calibration scheme for river forecasting models. Journal of Hydrometeorology. https://doi.org/10.1175/1525-7541(2000)001<0524:AMACSF>2.0.CO;2.

Jeff Reback, Wes McKinney, jbrockmendel, Joris Van den Bossche, Tom Augspurger, Phillip Cloud, gfyoung, Sinhrks, Adam Klein, Matthew Roeschke, Simon Hawkins, Jeff Tratner, Chang She, William Ayd, Terji Petersen, Marc Garcia, Jeremy Schendel (2020). pandas-dev/pandas: Pandas 1.0.3 (v1.0.3). Zenodo. https://doi.org/10.5281/zenodo.3715232.

Keeley, J.E., Keeley, S.C., 1981. Post-fire regeneration of southern California chaparral. American Journal of Botany 68 (4), 524–530. https://doi.org/10.1002/j.1537-2197.1981.tb07796.x.

Keller, E.A., Valentine, D.W., Gibbs, D.R., 1997. Hydrological response of small watersheds following the Southern California Painted Cave Fire of June 1990. Hydrological Processes 11 (4), 401–414. https://doi.org/10.1002/(SICI)1099-1085(19970330)11:4<401::AID-HYP447>3.0.CO;2-P.

Kinoshita, A.M., Hogue, T.S., 2011. Spatial and temporal controls on post-fire hydrologic recovery in Southern California watersheds. Catena 87 (2), 240–252. https://doi.org/10.1016/j.catena.2011.06.005.

Kinoshita, A.M., Hogue, T.S., 2015. Increased dry season water yield in burned watersheds in Southern California. Environmental Research Letters 10 (1), 014003. https://doi.org/10.1088/1748-9326/10/1/014003.

Kohli, G., Lee, C.M., Fisher, J.B., Halverson, G., Variano, E., Jin, Y., Carney, D., Wilder, B. A., Kinoshita, A.M., 2020. ECOSTRESS and CIMIS: A Comparison of Potential and Reference Evapotranspiration in Riverside County, California. Remote Sensing 12 (24), 4126. https://doi.org/10.3390/rs12244126.

Lentile, L.B., Morgan, P., Hudak, A.T., Bobbitt, M.J., Lewis, S.A., Smith, A.M., Robichaud, P.R., 2007. Post-fire burn severity and vegetation response following eight large wildfires across the western United States. Fire Ecology 3 (1), 91–108. https://doi.org/10.4996/fireecology.0301091.

Li, Y.i., Horton, R., Ren, T., Chen, C., 2010. Prediction of annual reference evapotranspiration using climatic data. Agricultural Water Management 97 (2), 300–308.

Ma, Q., Bales, R.C., Rungee, J., Conklin, M.H., Collins, B.M., Goulden, M.L., 2020. Wildfire controls on evapotranspiration in California's Sierra Nevada. Journal of Hydrology 590, 125364. https://doi.org/10.1016/j.jhydrol.2020.125364.

Mathews, L.E., Kinoshita, A.M., 2020. Vegetation and Fluvial Geomorphology Dynamics after an Urban Fire. Geosciences 10 (8), 317. https://doi.org/10.3390/geosciences10080317.

Mayor, A.G., Bautista, S., Llovet, J., Bellot, J., 2007. Post-fire hydrological and erosional responses of a Mediterranean landscpe: Seven years of catchment-scale dynamics. Catena 71 (1), 68–75. https://doi.org/10.1016/j.catena.2006.10.006.

Melton, F.S., Huntington, J., Grimm, R., Herring, J., Hall, M., Rollison, D., Erickson, T., Allen, R., Anderson, M., Fisher, J.B., Kilic, A., Senay, G.B., Volk, J., Hain, C., Johnson, L., Ruhoff, A., Blankenau, P., Bromley, M., Carrara, W., Daudert, B., Doherty, C., Dunkerly, C., Friedrichs, MacKenzie, Guzman, A., Halverson, G., Hansen, J., Harding, J., Kang, Y., Ketchum, D., Minor, B., Morton, C., Ortega-Salazar, S., Ott, T., Ozdogan, M., ReVelle, P.M., Schull, M., Wang, C., Yang, Y., Anderson, R.G., 2021. OpenET: Filling a critical data gap in water management for the western united states. JAWRA Journal of the American Water Resources Association. https://doi.org/10.1111/1752-1688.12956.

McKay, L., Bondelid, T., Dewald, T., Rea, A., Johnston, C., Moore, R., 2015. NHDPlus version 2: user guide (data model version 2.1). Horizon Systems.

Montes-Helu, M.C., Kolb, T., Dore, S., Sullivan, B., Hart, S.C., Koch, G., Hungate, B.A., 2009. Persistent effects of fire-induced vegetation change on energy partitioning and evapotranspiration in ponderosa pine forests. agricultural and forest meteorology 149 (3-4), 491–500. https://doi.org/10.1016/j.agrformet.2008.09.011.

Neary, D. G., Ryan, K. C., & DeBano, L. F. (2005). Wildland fire in ecosystems: effects of fire on soils and water. *Gen. Tech. Rep. RMRS-GTR-42-vol. 4. Ogden, UT: US Department of Agriculture, Forest Service, Rocky Mountain Research Station. 250 p., 42*. https://doi.org/10.2737/RMRS-GTR-42-V4.

Nolan, R.H., Lane, P.N., Benyon, R.G., Bradstock, R.A., Mitchell, P.J., 2014. Changes in evapotranspiration following wildfire in resprouting eucalypt forests. Ecohydrology 7 (5), 1363–1377. https://doi.org/10.1002/eco.1463.

Obrist, D., Yakir, D., Arnone III, J.A., 2004. Temporal and spatial patterns of soil water following wildfire-induced changes in plant communities in the Great Basin in Nevada. Plant and Soil 262 (1/2), 1–12. https://doi.org/10.1023/B:PLSO.0000037026.93675.a2.

Parsons, A., Robichaud, P.R., Lewis, S.A., Napper, C., Clark, J.T., 2010. Field guide for mapping post-fire soil burn severity. USDA Forest Service - General Technical Report RMRS-GTR. https://doi.org/10.2737/RMRS-GTR-243.

Peel, M.C., Finlayson, B.L., McMahon, T.A., 2007. Updated world map of the Köppen-Geiger climate classification. Hydrology and Earth System Sciences 11 (5), 1633–1644. https://doi.org/10.5194/hess-11-1633-200710.5194/hess-11-1633-2007-supplement.

Poon, P.K., Kinoshita, A.M., 2018. Spatial and temporal evapotranspiration trends after wildfire in semi-arid landscapes. Journal of Hydrology 559, 71–83. https://doi.org/10.1016/j.jhydrol.2018.02.023.

Prater, M.R., DeLucia, E.H., 2006. Non-native grasses alter evapotranspiration and energy balance in Great Basin sagebrush communities. Agricultural and Forest Meteorology 139 (1-2), 154–163.

Savoca, M. E., Senay, G. B., Maupin, M. A., Kenny, J. F., & Perry, C. A. (2013). Actual Evapotranspiration Modeling Using the Operational Simplified Surface Energy Balance (SSEBop) Approach. *U.S Geologica Survey Scientific Investigations Report 2013–5126*.

Soulis, K.X., Generali, K.A., Papadaki, C., Theodoropoulos, C., Psomiadis, E., 2021. Hydrological Response of Natural Mediterranean Watersheds to Forest Fires. Hydrology 8 (1), 15. https://doi.org/10.3390/hydrology8010015.

Taylor, A.H., Trouet, V., Skinner, C.N., 2008. Climatic influences on fire regimes in montane forests of the southern Cascades, California, USA. International Journal of Wildland Fire 17 (1), 60–71. https://doi.org/10.1071/WF07033.

Vieira, D.C.S., Fernández, C., Vega, J.A., Keizer, J.J., 2015. Does soil burn severity affect the post-fire runoff and interrill erosion response? A review based on meta-analysis of field rainfall simulation data. Journal of Hydrology 523, 452–464. https://doi.org/10.1016/j.jhydrol.2015.01.071.

Vo, V.D., Kinoshita, A.M., 2020. Remote sensing of vegetation conditions after post-fire mulch treatments. Journal of Environmental Management 260, 109993. https://doi.org/10.1016/j.jenvman.2019.109993.

USFS (2020, Jan). *Round table discussion*. Holy Fire Research Symposium at United States Forest Service Pacific Southwest Research Station, Riverside, California.

Uyeda, K.A., Stow, D.A., Riggan, P.J., 2015. Tracking MODIS NDVI time series to estimate fuel accumulation. Remote Sensing Letters 6 (8), 587–596. https://doi.org/10.1080/2150704X.2015.1063736.

Wagenbrenner, J.W., Ebel, B.A., Bladon, K.D., Kinoshita, A.M., 2021. Post-wildfire hydrologic recovery in Mediterranean climates: A systematic review and case study to identify current knowledge and opportunities. Journal of Hydrology 602, 126772. https://doi.org/10.1016/j.jhydrol.2021.126772.

Wenger, S. J., & Fowler, L. 2000. Protecting stream and river corridors: creating effective local riprian buffer ordinances.

WERT (Watershed Emergency Response Team). 2018. Holy Fire— Watershed Emergency Response Team final report, CA-RRU-100160. Sacramento, CA, p. 83. plus appendices.

Wilder, B.A., Lancaster, J.T., Cafferata, P.H., Coe, D.B.R., Swanson, B.J., Lindsay, D.N., Short, W.R., Kinoshita, A.M., 2021. An analytical solution for rapidly predicting post-fire peak streamflow for small watersheds in southern California. Hydrological Processes 35 (1). https://doi.org/10.1002/hyp.13976.

Wine, M.L., Cadol, D., Makhnin, O., 2018. In ecoregions across western USA streamflow increases during post-wildfire recovery. Environmental Research Letters 13 (1), 014010. https://doi.org/10.1088/1748-9326/aa9c5a.

Wittenberg, L., Malkinson, D., Beeri, O., Halutzy, A., Tesler, N., 2007. Spatial and temporal patterns of vegetation recovery following sequences of forest fires in a Mediterranean landscape, Mt. Carmel Israel. Catena 71 (1), 76–83. https://doi.org/10.1016/j.catena.2006.10.007.

Wohlgemuth, P. (2016, March). Long-term hydrologic research on the San Dimas Experimental Forest, southern California: Lessons learned and future directions. In C. E. Stringer, K. W. Krauss, J. S. Latimer (Eds.), Headwaters to estuaries: Advances in watershed science and management-Proceedings of the Fifth Interagency Conference on Research in the Watersheds. North Charleston, SC. e-General Technical Report SRS-211. Asheville, NC: US Department of Agriculture Forest Service, Southern Research Station. 302 p. (Vol. 211, pp. 227–232).

World Meteorological Organization. (2012). Standardized Precipitation Index User Guide (M. Svoboda, M. Hayes and D. Wood). *WMO-No. 1090* ©.

World Weather & Climate Information. (2022). Average monthly hours of sunshine in Los Angeles (California), United States of America. Retrieved March 9, 2022, from https://weather-and-climate.com/average-monthly-hours-Sunshine,Los-Angeles,United-States-of-America.